

Figure S1

Figure S1. Age-related changes in alveolar macrophage transcriptomes persist during influenza A infection in mice. Relates to Figure 1.

(A) Genetic validation of gating strategy for isolation of alveolar type 2 cells (AT2) from mice.

Single cell suspensions were prepared from the lungs of BAC transgenic mice expressing GFP

driven by the Surfactant protein C (*Sftpc*) promoter (*Tg-SFTPC-H2B-GFP*) and analyzed via

flow cytometry. Epithelial cells were identified as singlets/live/CD45-negative/CD31-

negative/EpCAM-positive cells and further subdivided based on EpCAM and MHC II expression.

Gate R1: EpCAM-high MHC II-negative, Gate R2: EpCAM-high MHC II-positive and Gate R3:

EpCAM-intermediate MHC II-positive. Over 95% of cells in gate R3 were positive for the *Sftpc*

promoter-driven GFP reporter and this gate was used to identify AT2 cells during conventional

flow sorting.

(B) Venn diagram shows overlap between differentially expressed genes between young and

old tissue resident alveolar macrophages in this study (Fig. 1C) and those reported by Wong et.

al., 2017.

(C) Venn diagram shows overlap between differentially expressed genes between young adult

and old naïve and influenza A-treated mice. A hypergeometric test was used to evaluate the

statistical significance for overlap.

(D) Volcano plots showing differentially expressed genes (FDR $q < 0.05$) between young adult

and old mice before and after infection with influenza A virus in alveolar macrophages and AT2

cells.

(E) tSNE plot shows representative marker genes for alveolar macrophages in young adult and

old mice.

(F) tSNE plot shows representative marker genes for AT2 cells in young adult and old mice.

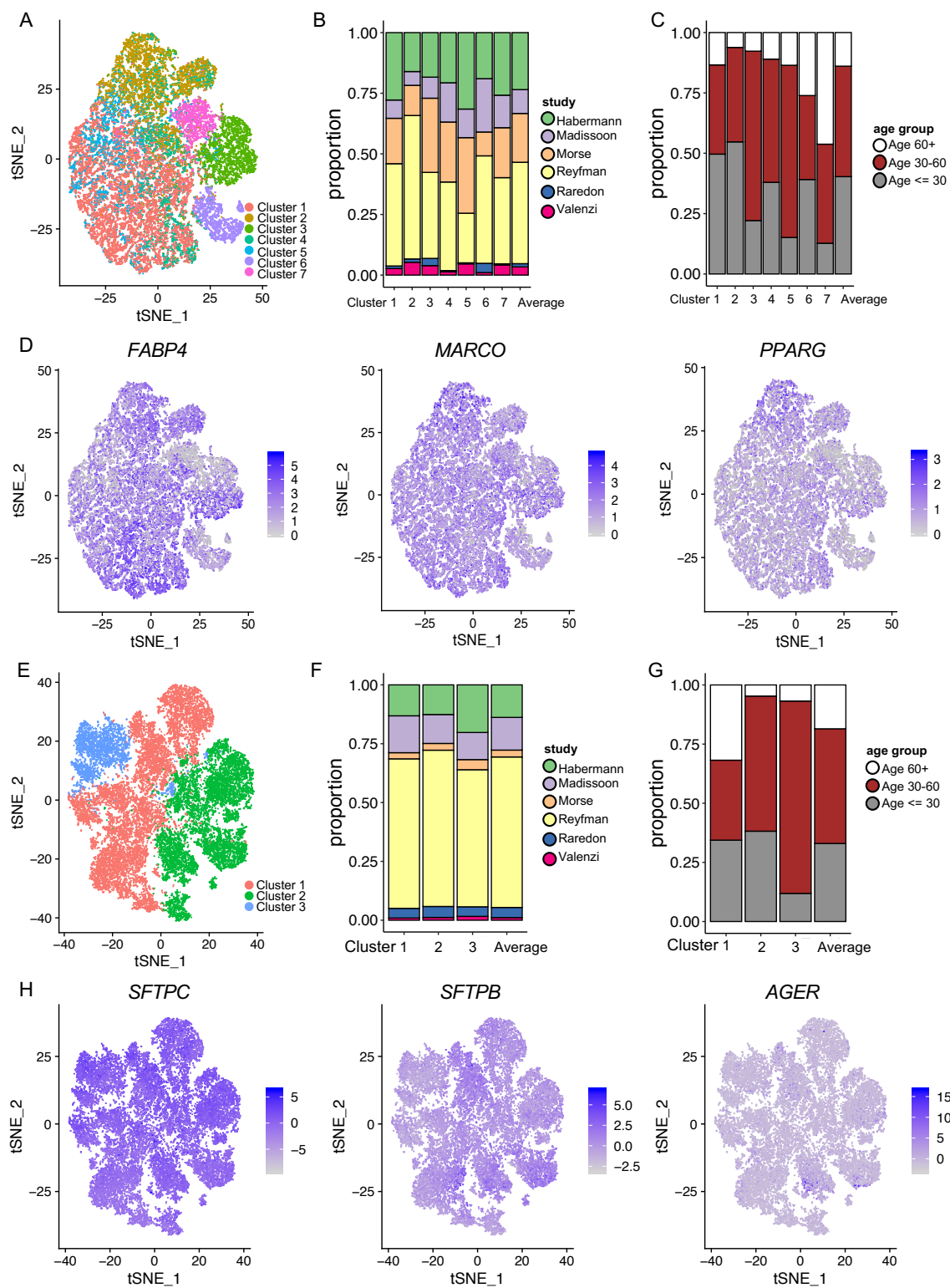


Figure S2

Figure S2. Integrated analysis of single cell RNA-Seq data obtained from the normal human lung reveals uniform changes in the transcriptome of alveolar macrophages with age. Relates to Figure 2.

(A) t-SNE plot shows clustering of alveolar macrophages from the six studies.

(B) Barplot showing contributions of alveolar macrophages from the six studies to the clusters.

(C) Barplot showing contributions of alveolar macrophages from individuals within chronological age tertiles to each cluster.

(D) Feature plots demonstrate distribution of canonical alveolar macrophage marker genes across clusters.

(E) t-SNE plot shows clustering of AT2 cells from the six studies.

(F) Barplot showing contributions of AT2 cells from the six studies to the clusters.

(G) Barplot showing contributions of AT2 cells from individuals within chronological age tertiles to each cluster.

(H) Feature plots demonstrate distribution of canonical alveolar type 2 (*SFTPC*, *SFTPB*) and alveolar type 1 cell (*AGER*) marker genes across clusters.

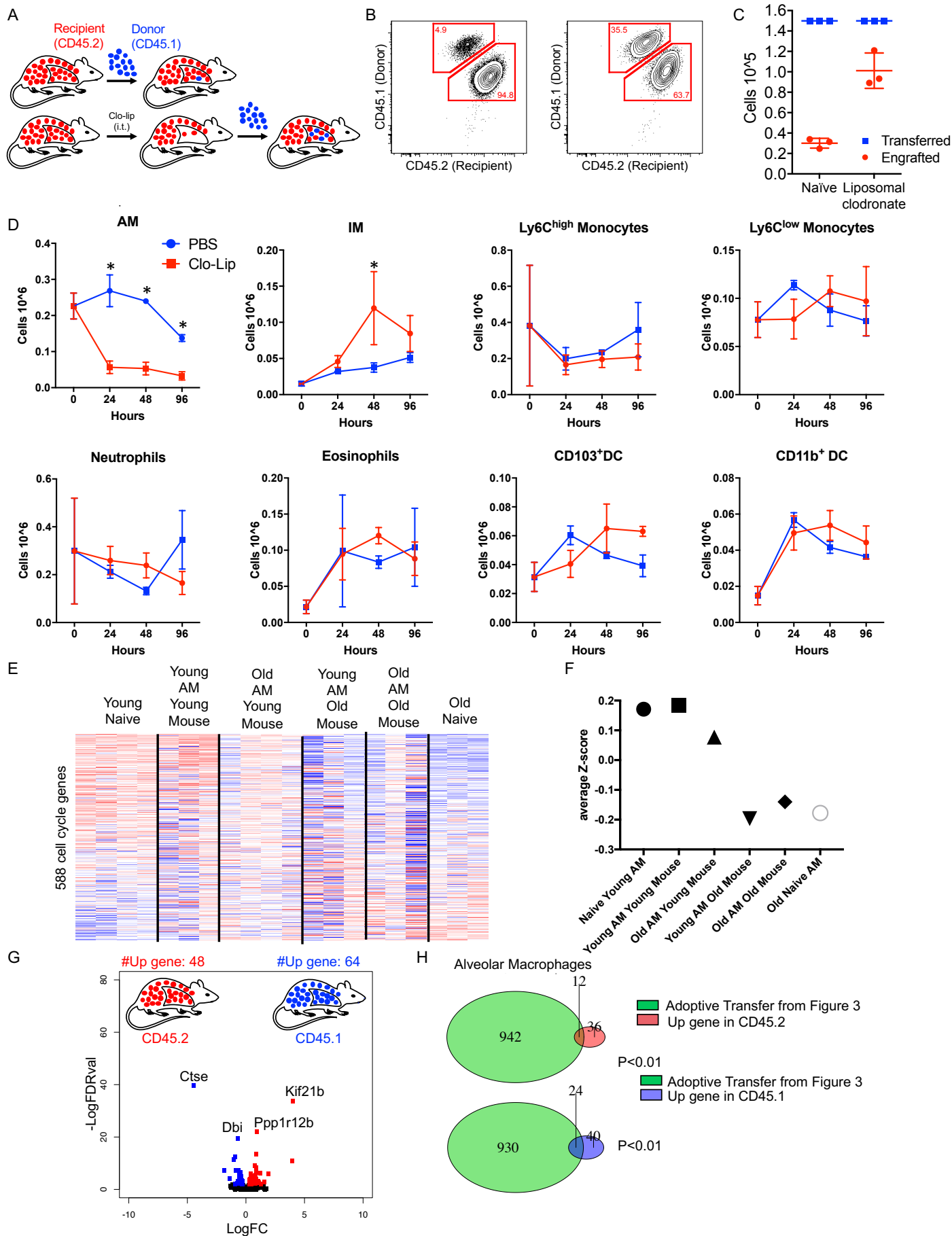


Figure S3

Figure S3. Age-related transcriptomic changes in tissue-resident alveolar macrophages are not cell autonomous.

(A) Schematic design of heterochronic adoptive transfer experiments with or without intratracheal liposomal clodronate.

(B) Representative flow cytometry plots from untreated and liposomal clodronate-treated CD45.2 mice (25 μ L, intratracheally) before the adoptive transfer of 1.5×10^5 TRAM from CD45.1 mice.

(C) Quantification of adoptively transferred TRAM 60 days after adoptive transfer (n=3 mice per group). $P < 0.05$ for engrafted group. Wilcoxon test.

(D) The number of immune cells measured in the single cell suspension prepared from the lung using flow cytometry 24, 48 and 96 hours after liposomal clodronate treatment (n=2-4 mice per group). * $P < 0.05$ for comparison between untreated and liposomal clodronate treated animals (Student's t-test).

(E) Heatmap showing the expression of cell cycle-related genes in TRAM 60 days after heterochronic adoptive transfer into young or old mice.

(F) Average Z scores for the cell cycle genes in each of the columns in (E).

(G) Volcano plot showing differentially expressed genes between TRAM from the lungs of CD45.1 or CD45.2 mice (FDR $q < 0.01$) (see Table S4 for full list of genes).

(H) Venn diagram shows overlap between differentially expressed genes in CD45.1/CD45.2 TRAM and genes differentially expressed in heterochronic adoptive transfer experiments (Refers to Figure 3D).

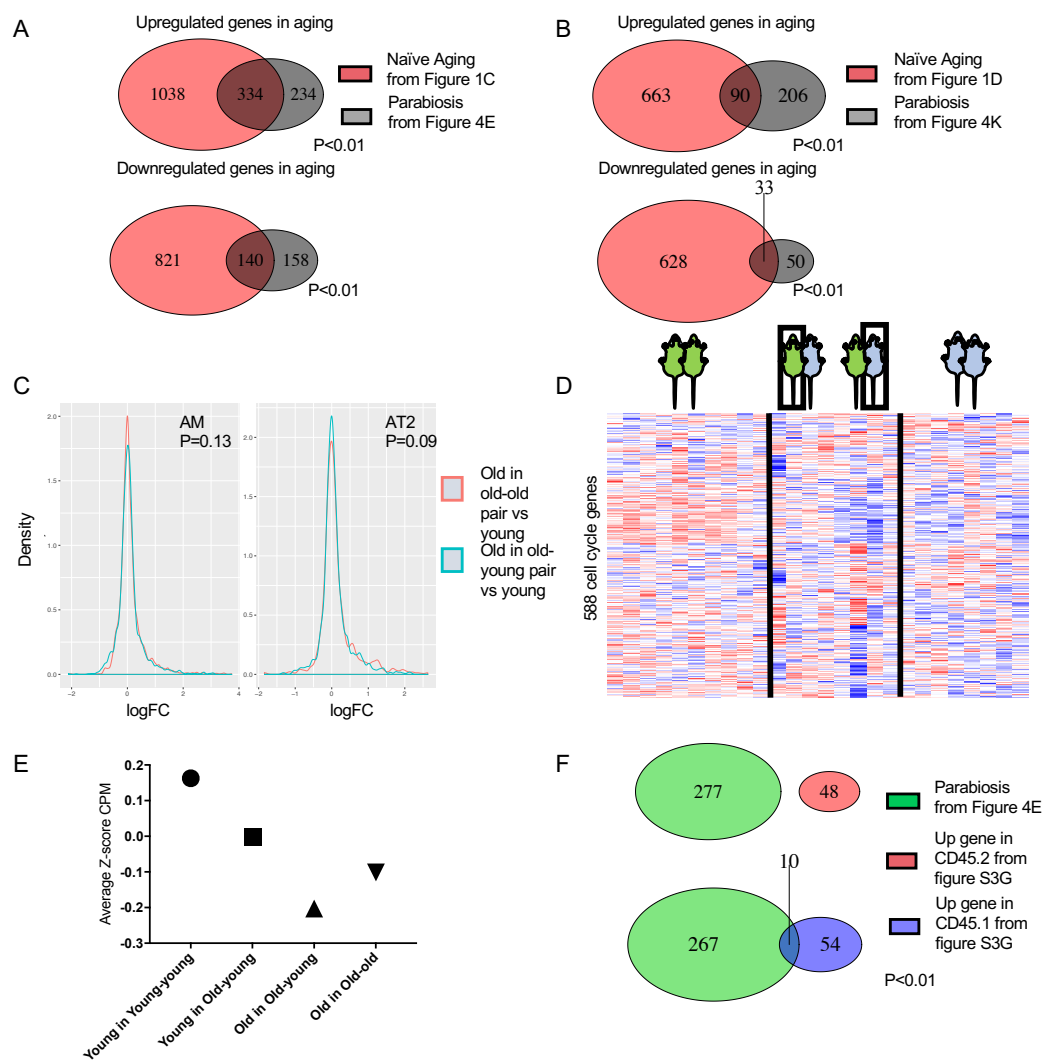


Figure S4

Figure S4. Heterochronic parabiosis does not reverse age-related transcriptomic changes in tissue-resident alveolar macrophages or alveolar type 2 cells.

(A) Venn diagram showing overlap of differentially expressed genes in young/young compared with old/old parabiont pairs and differentially expressed genes in TRAM identified between young adult (4-6 month) and old (18-24 month) mice (from Fig. 1C). Hypergeometric test.

(B) Venn diagram showing overlap of differentially expressed genes in young/young compared with old/old parabiont pairs and differentially expressed genes in AT2 cells (from Fig. 1D). Hypergeometric test.

(C) Distribution of log-fold change showing no significant difference ($p > 0.05$ by Wilcoxon rank sum test) for differentially expressed genes in TRAM and AT2 identified between young adult and old mice (from Fig. 1) and heterochronic parabiont pairs.

(D) Heatmap showing the lack of change in expression of cell cycle-related genes (from Fig. S3E) in TRAM between old and young adult mice with isochronic or heterochronic parabiont pairs.

(E) Average Z scores for the cell cycle genes for each of the columns in (D).

(F) Venn diagram showing overlap of differentially expressed genes in TRAM from parabionts in young/young compared with old/old pairs with differentially expressed genes (with FDR < 0.01) in TRAM from CD45.1 and CD45.2 mice (from Fig. S3G). Hypergeometric test.

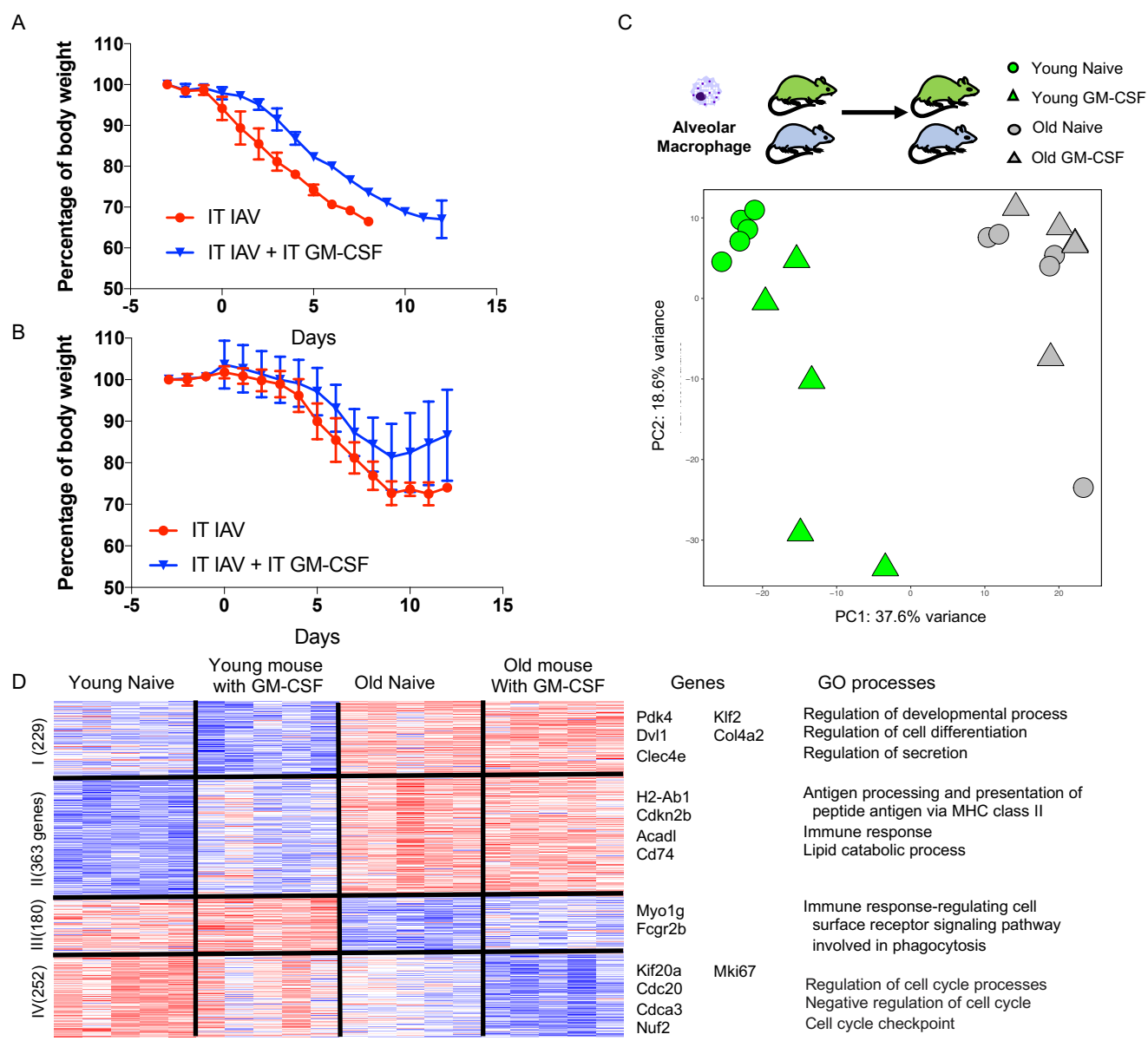


Figure S5

Figure S5. The aging microenvironment confers resistance to GM-CSF signaling in alveolar macrophages.

(A) Daily weight for old mice infected influenza A virus (A/WSN/33), 25 pfu/animal with (n=5) or without (n=4) intratracheally administered GM-CSF. $P=0.0007$ between two groups. Two-way ANOVA test.

(B) Daily weight loss curve for young adult mice with or without (both n=5) intratracheally administered GM-CSF. All mice received influenza A virus (A/WSN/33), 25 pfu/animal. $P=0.15$ between two groups. Two-way ANOVA test.

(C) Young adult (4-6 month) and old (18-24 month) mice were treated with exogenous GM-CSF (5 mg/kg day -3 and day 0) intratracheally and TRAM were harvested 14 days later for RNA-Seq. PCA plot of transcriptomes of TRAM from animals in the four conditions.

(D). Heatmap shows k-means clustering of differentially expressed genes in TRAM ($FDR < 0.01$ in ANOVA-like test) between old and young mice with or without treatment with GM-CSF. Selected genes and GO biological processes for each cluster are highlighted (see also table S16).

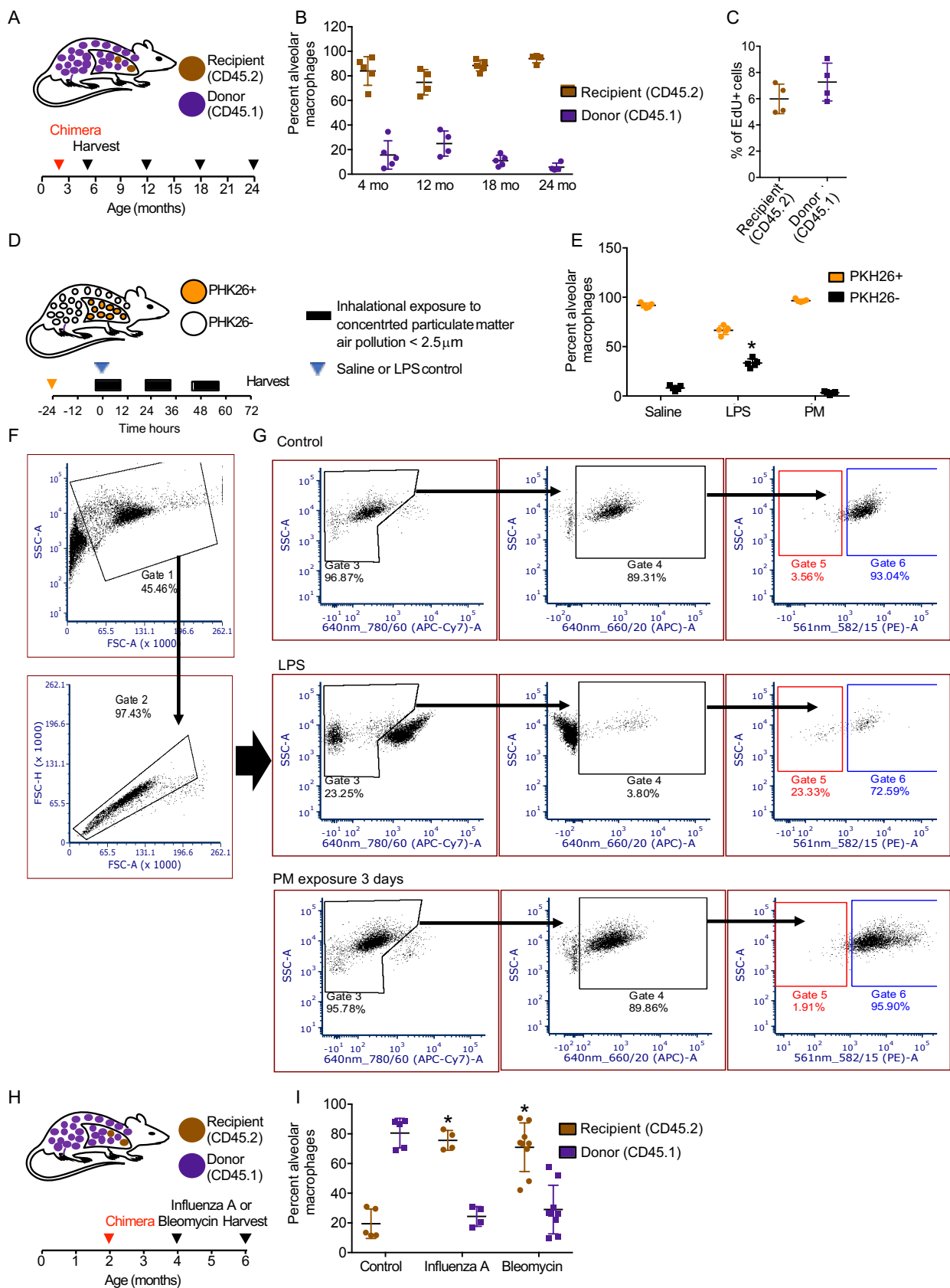


Figure S6

Figure S6. Tissue-resident alveolar macrophages represent a stable population that persists over the lifespan in the absence of severe lung injury.

(A) Schematic of the experimental design for (B,C). Bone marrow chimeric mice with thoracic shielding were generated from CD45.1 donors and CD45.2 recipients at 8 weeks of age and then harvested at the ages indicated.

(B) The percentage of monocyte-derived alveolar macrophages (MoAM, CD45.1) or TRAM (CD45.2) over the lifespan. Differences in the percentage of cells between ages were not significant (one-way ANOVA with Bonferroni correction, $n=3-5$ per time point).

(C) Percentage of EdU+ cells in MoAM (CD45.1) and TRAM (CD45.2) one day after a single pulse of EdU was administered (6 months of age). $N=4$ mice per group. $P>0.05$, student's t-test.

(D) Alveolar macrophages were labeled by intratracheal administration of PKH26 in vivo. After 24 hours, animals were treated intratracheally with PBS (50 mL), LPS (1 mg/kg in 50 mL PBS) or were exposed to concentrated particulate matter (PM) air pollution (6 hours of exposure $\sim 100-120$ mg/m³, 6 hours daily for 3 consecutive weekdays). Concentrations of particles are estimates based on particle measures from the inlet and outlet of the concentrator and reported ambient PM_{2.5} measures at a nearby Environmental Protection Agency monitoring station.

(E) Percentage of alveolar macrophages that were labeled (PKH26+) or unlabeled (PKH26-) after exposure to PBS, LPS or concentrated ambient PM air pollution via inhalation 6 hours daily for three consecutive weekdays. All mice were harvested after three days of exposure. One-way ANOVA with Bonferroni correction, $n=5$ per group, * indicates $P<0.05$ for comparison with control.

(F) Gating strategy to identify alveolar macrophages in bronchoalveolar lavage fluid via flow cytometry.

(G) Representative flow cytometry plots of bronchoalveolar lavage fluid from a control, LPS and PM-treated animal.

1 (H) Schematic showing shielded chimeric mice (4 months of age) were treated intratracheally
2 with influenza A virus (A/WSN/33) or intratracheal bleomycin and then harvested 60 days later.
3 (I) MoAM (CD45.1) and TRAM (CD45.2) were quantified by flow cytometry 60 days after
4 infection with influenza A virus (A/WSN/33) or intratracheal administration of bleomycin. Control
5 mice were not treated. * indicates $P < 0.05$ for comparison with untreated mice (paired t-test).
6 N=4-9 mice per group.

7

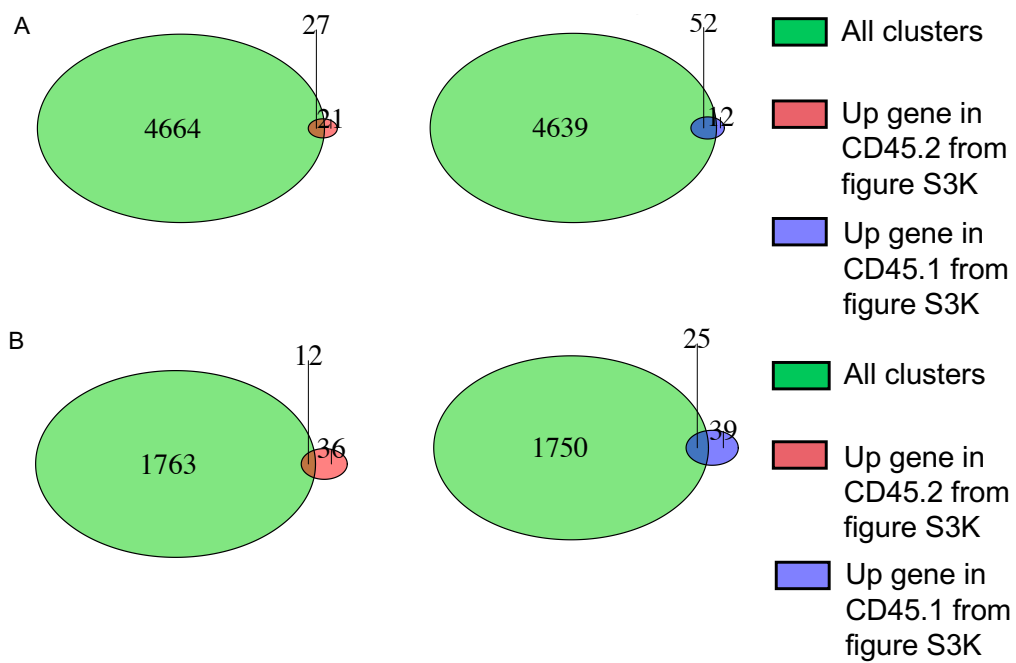


Figure S7

Figure S7. Differences between CD45.1/CD45.2 strains do not explain differential gene expression in tissue-resident alveolar macrophages and monocyte-derived alveolar macrophages from aged shielded chimeric mice.

(A) Venn diagram showing overlap between all differentially expressed genes in TRAM and MoAM from shielded chimeras in aging (See Fig. 6A) with those differentially expressed in TRAM from untreated CD45.1 and CD45.2 mice (from Fig. S3G). Hypergeometric test.

(B) Venn diagram showing overlap between differentially expressed genes in Clusters IV and V of Fig. 6A (comparison of TRAM and MoAM in aging shielded chimeras) with those differentially expressed in TRAM from untreated CD45.1 and CD45.2 mice (from Fig. S3G). Hypergeometric test.

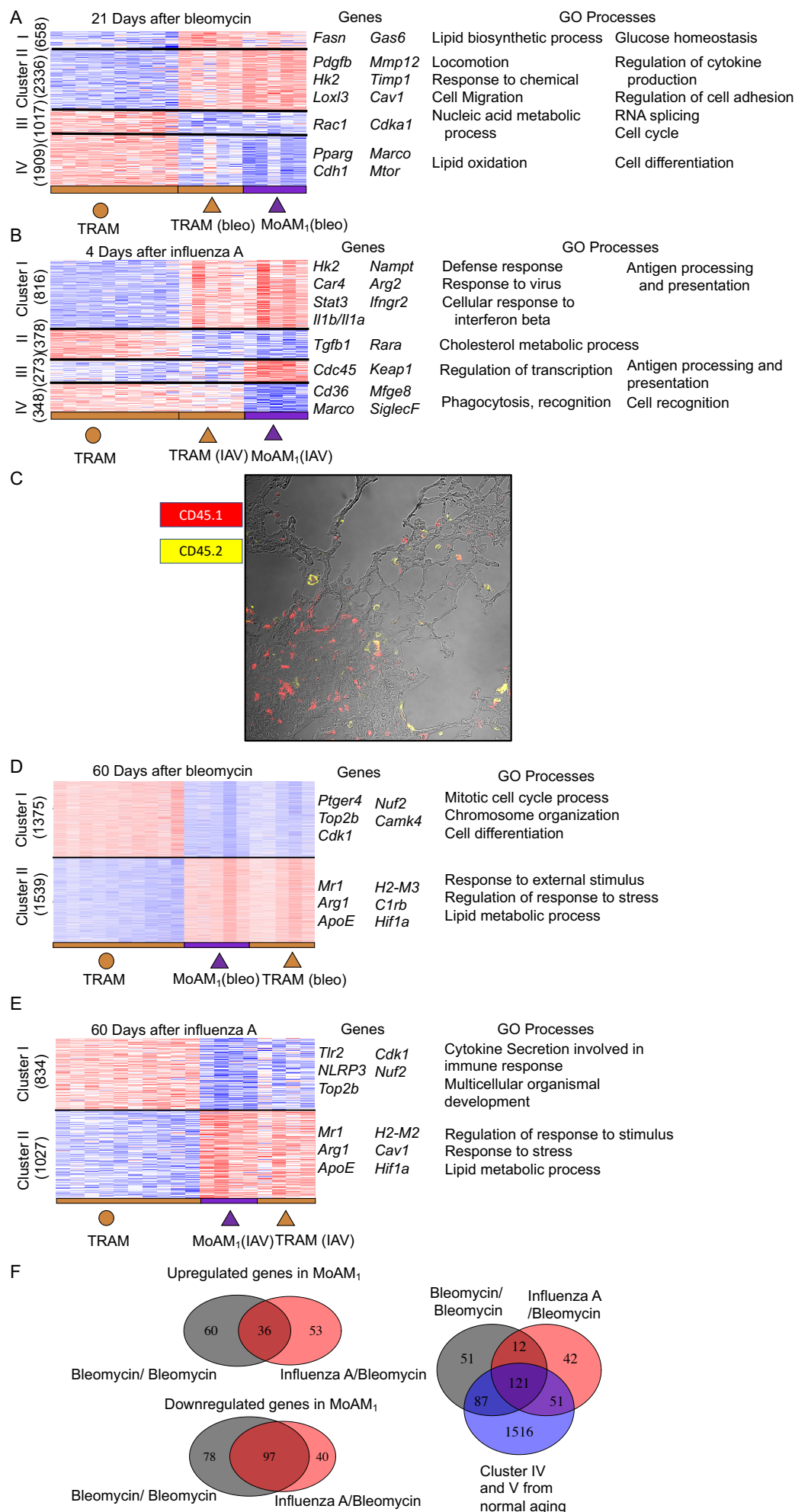


Figure S8

Figure S8. During injury, monocyte-derived alveolar macrophages show enhanced inflammatory gene expression after influenza A infection and enhanced fibrotic gene expression after bleomycin exposure when compared with tissue-resident alveolar macrophages. Monocyte-derived alveolar macrophages and tissue-resident alveolar macrophages become increasingly similar during the resolution of lung injury.

(A) Heatmap shows k-means clustering of differentially expressed genes between naïve TRAM, TRAM 21 days after bleomycin-induced lung injury, and recruited MoAM collected at the same time points (FDR $q < 0.01$ in ANOVA-like test). Representative genes and GO processes are shown on the right. See also Table S20.

(B) Heatmap shows k-means clustering of differentially expressed genes between naïve TRAM, TRAM 4 days after influenza A-infection, and recruited Mo-AM at the same time (FDR $q < 0.01$ in ANOVA like test). Representative genes and GO processes are shown on the right. See also Table S21.

(C) Lung sections from shielded chimeric mice 21 days after the administration of bleomycin were analyzed using immunofluorescent microscopy with antibodies against CD45.2 to label TRAM (yellow) or CD45.1 to label MoAM (red). As demonstrated in the representative section, CD45.1 MoAM were disproportionately represented in areas of injury/fibrosis compared to areas that were relatively free of fibrosis.

(D) Heatmap shows k-means clustering of differentially expressed genes (FDR < 0.01) in TRAM and MoAM retained after bleomycin-induced pulmonary fibrosis. Naïve TRAM are included as a comparison. Representative genes and GO biological processes are shown on the right. See also table S22.

(E) Heatmap shows k-means clustering of differentially expressed genes (FDR < 0.01) in TRAM and MoAM retained after influenza A-induced pneumonia. Naïve TRAM are included as a comparison. Representative genes and GO processes are shown on the right. See also table S23.

1 (F) Venn diagram shows overlap between genes differentially expressed ($FDR < 0.01$) between
2 TRAM and MoAM recruited in response to historic bleomycin or influenza A infection after a
3 second injury with bleomycin and the differences observed between TRAM and MoAM in
4 normal aging (refers to Fig. 6A). P value for overlap < 0.01 . Hypergeometric test.

5

6

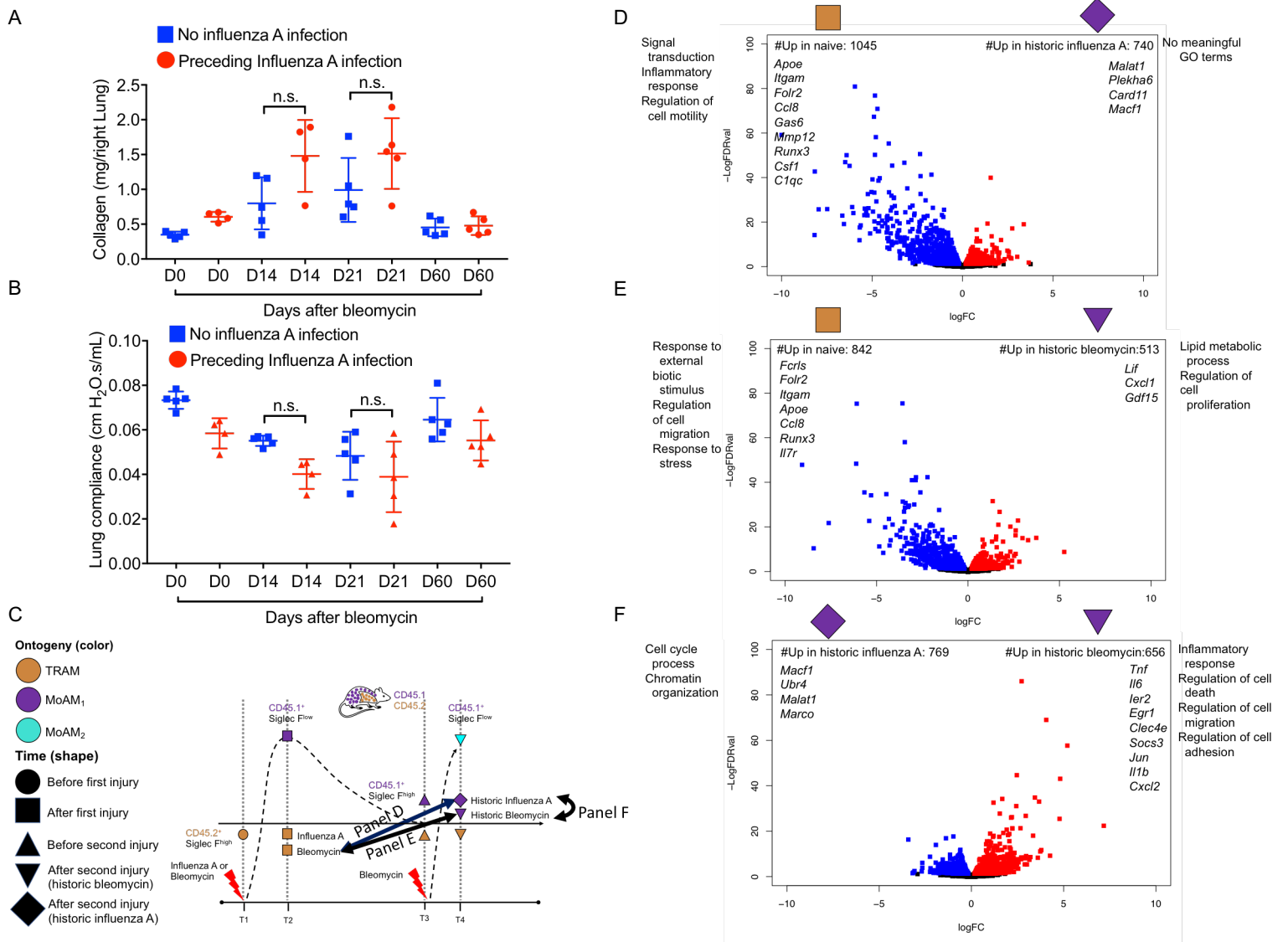


Figure S9

Figure S9. Tissue-resident alveolar macrophages demonstrate immune tolerance irrespective of ontogeny.

(A) Collagen levels (picosirius red precipitation) measured in mice after a single bleomycin exposure with or without a preceding influenza infection (n=4-5 mice per group). FDR $q > 0.05$ after multiple comparison adjustment.

(B) Lung compliance measured in mice after a single bleomycin exposure with or without preceding influenza A infection (n=4-5 mice per group). FDR $q > 0.05$ after multiple comparison adjustment.

(C) Schematic for experimental design for panel D-F . Pairwise comparisons described in panels D through F are indicated by double arrow.

(D) Volcano plot comparing TRAM during the first injury (bleomycin) and MoAM recruited after historic infection with influenza A virus, both re-challenged with bleomycin (FDR $q < 0.05$).

Selected differentially expressed genes and GO biological processes are shown. See Table S24 for a full list of genes.

(E) Volcano plot comparing TRAM during the first injury (bleomycin) and MoAM recruited after historic exposure to bleomycin, both re-challenged with bleomycin (FDR $q < 0.05$). Selected differentially expressed genes and GO biological processes are shown. See Table S24 for a full list of genes.

(F) Volcano plot comparing MoAM recruited after historic exposure to bleomycin or infection with influenza A virus, both re-challenged with bleomycin (FDR $q < 0.05$). Selected differentially expressed genes and GO biological processes are shown. See Table S24 for a full list of genes.